

Thermophysical, dielectric, and electro-optic properties of nematic liquid crystal droplets confined to a thermoplastic polymer matrix

Mourad Boussoualem and Frédérick Roussel*

Laboratoire de Thermophysique de la Matière Condensée, Equipe de l'UMR CNRS 8024, Université du Littoral-Côte d'Opale, MREI, 59140 Dunkerque, France

Mimoun Ismaili

Laboratoire de Dynamique et Structure des Matériaux Moléculaires, UMR CNRS 8024, Université des Sciences et Technologies de Lille, P5, 59655 Villeneuve d'Ascq, France

(Received 24 June 2003; published 4 March 2004)

The thermophysical, dielectric and electro-optic properties of polymer-dispersed liquid crystal (PDLC) films made of monodisperse polystyrene (PS) and 4-*n*-pentyl-4'-cyanobiphenyl (5CB) are investigated by polarized optical microscopy, differential scanning calorimetry, ac impedance analysis, and forward transmittance measurement technique. The PS-5CB system exhibits an upper critical solution temperature (UCST) shape phase diagram with a wide isotropic+isotropic (*I+I*) miscibility gap between the isotropic and nematic+isotropic (*N+I*) regions. An absorption domain in the dielectric spectrum of PDLC films was clearly observed at low frequency, and unambiguously assigned to the confined liquid crystalline phase in both nematic and isotropic states. The correlation between the dielectric and electro-optical results for PS-5CB (30:70) samples has shown that in the vicinity of the low frequency absorption domain (~ 200 Hz at $T=25^\circ\text{C}$), a drastic decrease in the optical transmittance of the film occurs. This phenomenon can be related to an interfacial polarization process resulting from a charge accumulation at the droplet-polymer interface (Maxwell-Wagner-Sillars effect).

DOI: 10.1103/PhysRevE.69.031702

PACS number(s): 61.30.Pq, 64.75.+g, 77.22.Gm, 42.70.Df

I. INTRODUCTION

In the past decade, polymer dispersed-liquid crystals (PDLC) have found great interest because of their promising use in advanced optical device applications, such as large flexible displays, switchable windows, or paperlike displays for electronic books [1–4]. In their most common form, PDLC films consist of low molecular weight liquid crystals (LC) dispersed as micrometer-sized droplets within a solid polymer matrix. Among the main aspects governing the electro-optical performances (e.g., transmission properties, drive voltage, switching times) of these materials are the concentration of LC, the morphology of the films, the anchoring conditions of the LC at the polymer interface, and the dielectric properties of the composite in alternating electric fields [5–10]. It has been demonstrated that the phase behavior and the phase separation mechanism used to prepare PDLC strongly determine the morphology of the films [5,11–13]. The knowledge of the phase diagram of a polymer-LC system is then a prerequisite for any complete interpretation of the electro-optical characterization with respect to the film morphology of PDLC materials. Several theoretical works have been done to explain the local field effects, the electro-optical phase shift, and the field-dependent dielectric response of PDLC films. Two main approaches have been used which are based either on the Maxwell Garnett approximation [14,15] or on an effective

medium model [16]. Experimental dielectric studies of confined nematic LC phases have been performed in numerous materials such as membranes [17–19] or porous glasses [17,20–24], but only few reports have been devoted to PDLC systems [10,25,26]. A possible explanation may arise from the complexity of PDLC formulations for technological devices and/or the relatively high conductivity of their components [1,25,26]. Indeed, the contribution of the conductivity caused by mobile charge carriers often overlaps low frequency dielectric absorption domains which are usually assigned to interfacial effects. These effects are of main importance for heterogeneous materials such as PDLC, because they can strongly influence the electro-optical performances of PDLC display devices. Therefore, the goal of this paper is to investigate the dielectric properties of PDLC films in regard of their thermophysical and electro-optical behaviors. In order to account for the parameters influencing the electrical properties of PDLC materials, a model system based on a well-characterized monodisperse polystyrene (PS) and a pure liquid crystal [4-*n*-pentyl-4'-cyanobiphenyl (5CB)] has been chosen and investigated by polarized optical microscopy (POM), differential scanning calorimetry (DSC), ac impedance analysis, and forward transmittance measurement technique. The phase diagram covering a wide LC concentration range is established by POM and DSC, whereas the LC solubility limit in the polymer and the fractional amount of phase-separated LC are deduced from DSC data. Broad band dielectric spectroscopy is used to investigate the electrical behavior of homogeneous and phase-separated PS-5CB mixtures. The results are then compared to the electro-optical response (transmittance versus frequency of the applied voltage) of the same PDLC film.

*Corresponding author. Email address: Frederick.Roussel@purple.univ-littoral.fr

II. EXPERIMENT

The liquid crystal 4-*n*-pentyl-4'-cyanobiphenyl (5CB) was used during this work. 5CB (Aldrich, Saint Quentin-Fallavier, France) exhibits a nematic (*N*) phase between the crystalline (*Cr*) and isotropic (*I*) states in the temperature range 24.5–35.1 °C. 5CB is easily supercooled from the *N* state to –10 °C. PS was used as polymer matrix because it presents three main advantages compared to other thermoplastic compounds: (i) The dc conductivity of PS is very low ($\sigma_{dc} \approx 10^{-18} \text{ S cm}^{-1}$), as well as its ac conductivity ($\sigma_{ac} \approx 10^{-9} \text{ S cm}^{-1}$) [27]; (ii) The dielectric permittivity of PS remains unchanged ($\epsilon \sim 2.5$) in both temperature (25 °C–80 °C) and frequency (1 kHz–100 MHz) ranges of interest [27,28]; (iii) Well-characterized monodisperse PS ($M_w = 200\,000 \text{ g mol}^{-1}$, polydispersity $I_p = 1.05$) is commercially available (Aldrich, Saint Quentin-Fallavier, France). PS and 5CB with different LC compositions were dissolved in a common solvent [tetrahydrofuran (THF)] at 50 wt%. Mixtures were stirred mechanically for 12 h. Samples were prepared following a standard procedure for microscopy observations. A small amount of the mixture was cast on a clean glass slide, and the sample was left for 24 h to allow for a complete evaporation of the solvent (THF). Another glass slide was put on the top of the first one, and the dry sample was sandwiched between the two glass slides leading to an average POM cell thickness of 2–3 μm . For the DSC measurements, the samples were prepared by introducing a few drops of the initial mixture into aluminum DSC pans (diameter $\sim 4 \text{ mm}$). The low viscosity of the initial mixture rapidly led to the formation of a thin film in close contact to the pan bottom. After complete evaporation of the solvent, the DSC pan was weighted and the whole procedure was repeated until the introduction of ca. 3 mg of sample. Assuming that the density of the PS-5CB blends is close to 1 ($d_{PS} = 1.047$ and $d_{5CB} = 1.008$), the calculated film thickness was $\sim 60 \mu\text{m}$. For dielectric and electro-optic samples, the dried initial mixture in the isotropic state was introduced by capillarity into calibrated 50 μm transparent conducting (ITO) commercial cells (EHC, Japan) at $T = 70 \text{ }^\circ\text{C}$. After complete filling of the cell, the sample was cooled to room temperature at a rate of $-2 \text{ }^\circ\text{C min}^{-1}$. For a given PS-5CB mixture, both dielectric and electro-optical experiments were successively carried out on the same measurement cell.

The polarized optical microscopy (POM) studies were performed on a Leica DMRXP microscope equipped with a heating or cooling stage Linkam THMSE-600. Samples were heated at a rate of $2 \text{ }^\circ\text{C min}^{-1}$ from room temperature to 15° above the transition temperature leading to the isotropic phase. Samples were kept at this temperature for 5 min, then cooled to $T = 0 \text{ }^\circ\text{C}$ at a rate of $-2 \text{ }^\circ\text{C min}^{-1}$. Subsequently, a second heating cycle ($2 \text{ }^\circ\text{C min}^{-1}$) up to the isotropic state was carried out. The whole procedure was repeated twice, and at least two independent samples of the same composition were analyzed. Transition temperatures were recorded during the second heating ramp.

DSC measurements were performed on a Seiko DSC 220C calorimeter equipped with a liquid nitrogen system allowing cooling experiments. The DSC cell was purged with

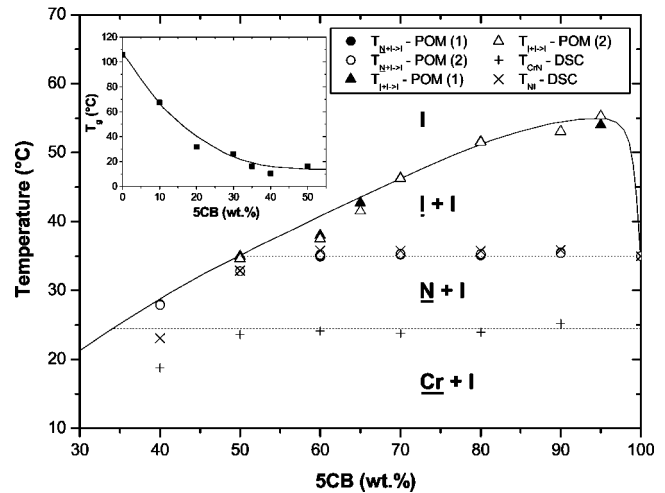


FIG. 1. Phase diagram of PS-5CB obtained from POM and DSC techniques. The open and filled symbols are averages of two series of samples from separate POM experiments. Cross and plus symbols are DSC data. Solid and dotted lines are guides to the eyes. T_{CrN} is the melting temperature of 5CB, $T_{(N+I) \rightarrow I}$ and T_{NI} represent the transition temperature of the phase separated liquid crystal between the nematic and isotropic states, and $T_{(I+I) \rightarrow I}$ is the isotropic+isotropic to isotropic transition temperature. The phase diagram exhibits four domains: Crystal+isotropic (*Cr*+*I*), Nematic+isotropic (*N*+*I*), Isotropic+Isotropic (*I*+*I*), and Isotropic (*I*), where *Cr*, *N*, and *I* refer to the phase-separated LC domains, and *I* is associated with the homogeneous polymer rich phase. Inset: Polymer glass transition temperature T_g vs LC weight fraction.

50 ml min^{-1} of nitrogen. Rates of $5 \text{ }^\circ\text{C min}^{-1}$ (heating) and $30 \text{ }^\circ\text{C min}^{-1}$ (cooling) were used in the temperature range $-100 \text{ }^\circ\text{C}$ to $+100 \text{ }^\circ\text{C}$. The temperature treatment consists first in cooling the samples prior to heating and cooling cycles. The peaks of the clearing points were used to determine the nematic-isotropic transition temperature T_{NI} . Typical DSC thermograms of PS-LC systems have already been reported elsewhere [29,30], and are not presented here again.

The real (ϵ') and imaginary (ϵ'') parts of the complex dielectric permittivity [$\epsilon^*(\omega) = \epsilon'(\omega) - j\epsilon''(\omega)$] of PS-5CB mixtures were recorded with a HP 4192A impedance or gain-phase analyzer generating a 100 mV sinusoidal voltage in the frequency range 5 Hz–13 MHz. Temperature control of the capacitor was achieved with a Mettler Toledo FP82HT-FP90 setup. The electro-optical (EO) properties of PDLC films were determined from time-resolved forward transmittance of a He-Ne laser beam passing through the film, while applying across the film a 1 kHz sinusoidal voltage modulated in amplitude by a triangular wave ($V_{pp} = 140 \text{ V}$, $1.67 \times 10^{-2} \text{ Hz}$) [31].

III. RESULTS AND DISCUSSION

A. Thermophysical properties

Figure 1 shows the phase diagram of PS-5CB mixtures in the form of temperature versus LC weight fraction. The symbols represent POM and DSC data as indicated in the figure caption, whereas solid and dotted lines are guides to the

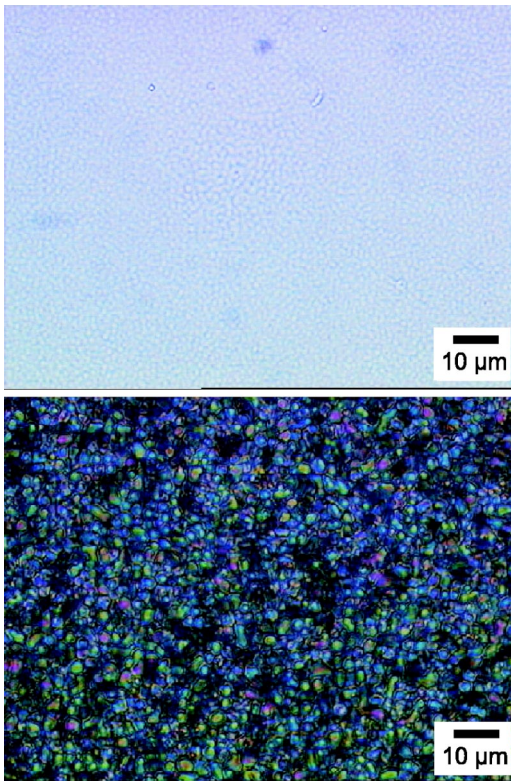


FIG. 2. Optical micrographs of PS-5CB (30:70). Bottom: $T = 25^\circ\text{C}$ ($N+I$) region (crossed polarizers mode $P \perp A$, magnification $\times 320$); top: $T = 40^\circ\text{C}$ ($I+I$) region ($P \parallel A$, magnification $\times 320$).

eyes. One can see a good agreement between the two series of samples from separate POM experiments. DSC data obtained for the nematic to isotropic transition temperature T_{NI} are also in good agreement with the POM measurements. It is worth noting that the DSC thermograms did not show the ($I+I$) to (I) transition [13,30]. This means that the existence of the ($I+I$) phase was evidenced by POM observations. The diagram exhibits an upper critical solution temperature (UCST) shape with four distinct regions. In the upper part of the phase diagram, the system exhibits a single isotropic (I) phase. When the temperature is lowered, a biphasic (isotropic+isotropic, $I+I$) region was observed (Fig. 2). With further lowering of temperature, an isotropic polymer-rich phase is in equilibrium with a nematic LC phase (Fig. 2). In the range of LC compositions above 50 wt% the ($N+I$) to ($I+I$) transition temperature is almost constant at about $T = 35^\circ\text{C}$, which corresponds approximately to the $N-I$ transition temperature of bulk 5CB. This observation indicates that the phase-separated NLC domains are essentially pure. In the lower part of the phase diagram, 5CB domains are in the crystalline state leading to a crystal + isotropic region ($Cr+I$). Between the circle and triangle symbols, the phase diagram exhibits a wide isotropic miscibility gap ($I+I$) showing the incompatibility between the polymer and the LC. It is interesting to note that the ($I+I$) domain covers a range of temperature up to 20°C near the critical point ($T_c \approx 54^\circ\text{C}$, $\phi_c \approx 95$ wt% 5CB) which is in good agreement with the phase diagrams of PS-LC blends

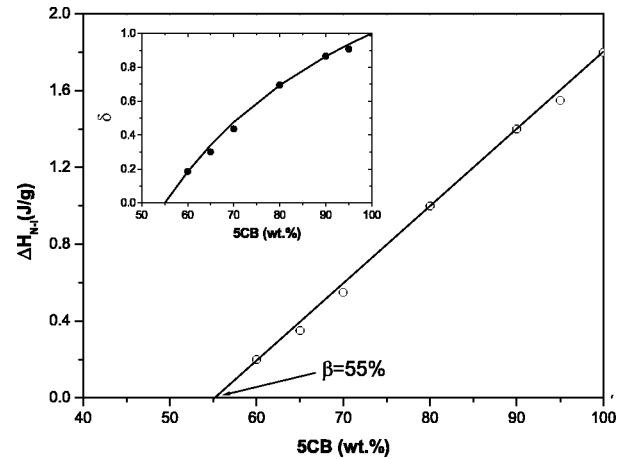


FIG. 3. Enthalpy changes at the nematic-isotropic transition vs 5CB content. The LC solubility limit β was determined by linear regression of the experimental data set. Inset: Dependence of the fractional amount of LC contained in the droplets (δ) on the LC concentration.

reported in the literature [29,30]. The inset of Fig. 1 displays the variation of the polymer glass transition temperature T_g as a function of the composition of 5CB indicating a sharp decrease from $T = 103^\circ\text{C}$ (T_g of pure PS) to about $T = 13^\circ\text{C}$ for PS-5CB (50:50) mixtures. Above this composition T_g remains almost constant due to the solubility limit of 5CB in PS. This decrease of T_g is due to the fact that the LC plays the role of plasticizer for the polymer [29,30].

The solubility limit β of the LC molecules in the polymer and the relative amount δ of LC in the nematic droplets are other interesting properties that can be deduced from the phase diagram and the thermodynamic quantities accessible from DSC data. β can be related to the enthalpy change at the nematic-isotropic transition ΔH_{NI} [13,30,32]:

$$P(x) = \frac{x - \beta}{100 - \beta}, \quad \text{with} \quad P(x) = \frac{\Delta H_{NI}(x)}{\Delta H_{NI}(\text{LC})}. \quad (1)$$

$P(x)$ represents the ratio of the nematic-isotropic transition enthalpy for a LC-polymer composite material to the equivalent value for pure LC. This expression is based on the following assumptions: (i) the LC in the droplets exhibits the same thermophysical behavior as in the bulk state; (ii) the amount of LC dissolved in the polymer is constant for LC concentrations $x \geq \beta$, and does not contribute to ΔH_{NI} ; (iii) T_{NI} values as a function of x remain unchanged. The effect of LC concentration on ΔH_{NI} is presented in Fig. 3. ΔH_{NI} increases linearly with x , validating the model given in Eq. (1). The LC solubility limit β was determined by linear regression of the experimental data set in Fig. 3 followed by calculating the x -axis intercept. The value of β was 55% which is comparable to other PS-LC mixtures such as PS-7CB [29] or PS-8CB [30]. ΔH_{NI} can be used to calculate δ_e , the LC fraction contained in the droplets [13,30,32]:

$$\delta_e = \frac{m_{LC}^D}{m_{LC}} = \left(1 + \frac{m_P}{m_{LC}}\right) P(x) = \left(\frac{100}{x}\right) P(x), \quad (2)$$

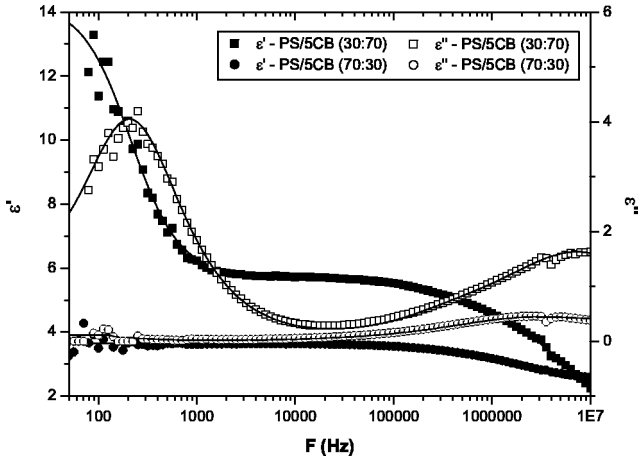


FIG. 4. Real (ϵ') and imaginary (ϵ'') parts of the complex permittivity of 50 μm thick PS-5CB (30:70) and PS-5CB (70:30) films in the frequency range 50 Hz–10 MHz at $T=25^\circ\text{C}$. The solid lines are Havriliak-Negami fit curves.

where m_{LC}^D represents the mass of LC included in the droplets, while m_P and m_{LC} are the masses of polymer and LC in the sample, respectively. Combining Eqs. 1 and 2 yields

$$\delta_c = \left(\frac{100}{x}\right) \left(\frac{x-\beta}{100-\beta}\right), \quad x \geq \beta. \quad (3)$$

Inset of Fig. 3 illustrates the dependence of δ on the LC concentration. The filled circles represent δ_e values determined for each composition by applying Eq. (2), whereas the solid line was calculated (δ_c) by using the previously mentioned β value and Eq. (3). At the miscibility limit, x is equal to β and δ is zero, consistent with Eq. (3). When x increases, δ_e increases rapidly. Experimental values and calculated curve are in good agreement.

B. Dielectric properties

Figure 4 shows the real (ϵ') and imaginary (ϵ'') parts of the complex permittivity of the PS-5CB(30:70) and PS-5CB(70:30) mixtures in the frequency range 50 Hz–10 MHz at $T=25^\circ\text{C}$. The Havriliak-Negami analysis [33,34] was applied for the quantitative interpretation of the dielectric data to determine the corresponding mean relaxation rates ($1/\tau_{max}$) and dielectric strengths [$\Delta\epsilon=(\epsilon_s-\epsilon_\infty)$] of the relaxation processes. In Fig. 4, the filled and open symbols are the experimental data whereas the solid lines are Havriliak-Negami fit curves. In the case of the PS-5CB(70:30) system (\circ and \bullet symbols), a relaxation mechanism is observed at high frequency, $\sim 4\text{--}6$ MHz. Recalling that a mixture including 30 wt % of 5CB is fully isotropic, i.e., homogeneous, at $T \geq 22^\circ\text{C}$ (see Fig. 1), the 5CB molecules dissolved in the PS matrix can be considered as single molecules randomly dispersed in an isotropic polymeric medium. Two types of relaxation processes may then arise which can be related to the “solute,” i.e., the LC molecules, or to the “matrix,” i.e., the PS chains. Walker *et al.* investigated the dielectric properties of rigid polar molecules (*p*-halobiphenyl, *p*-nitrobiphenyl, . . .) in a viscous molecular environment

(atic polystyrene matrix) [35]. This kind of molecules has in common with LC compounds a molecular dipole moment which lies along the main principal axis. These authors demonstrated that for elongated rigid polar molecules in-plane rotation is a favored mechanism because it involves less displacement of surrounding PS segments. Relaxation times and dielectric loss factors ϵ''_{max} were found in the range of $\sim 10^6$ Hz and 10^{-2} , respectively. The amplitude of the dielectric absorption is at least ten times smaller compared with our experimental data ($\epsilon''_{max} \approx 0.5$) indicating that another relaxation process related to the PS chains obviously occurs overlapping the relaxation mechanism corresponding to the in-plane rotation along the long molecular axis of the LC molecules. For a pure polymer, the dielectric relaxation mechanism observed above the glass transition is a segmental motion of the macromolecular chains commonly named α process. The relaxation rate of the α process measured for PS thin films (13–1940 nm) is typically in the frequency range of $10^{-3}\text{--}10^4$ Hz [36,37]. Compared to the value obtained for the PS-5CB (70:30) system [$1/\tau_{max} \sim (4\text{--}5) \times 10^6$ Hz], a difference of at least two orders of magnitude is observed. Recalling that the LC molecules act as a plasticizer for the polymer matrix (Sec. III A), the PS glass transition temperature is shifted at lower temperature, i.e., $T_g \approx 21^\circ\text{C}$ for PS-5CB (70:30). This plasticizing effect may also change the relaxation frequency range of the α process. In order to decipher the assignment of the dielectric spectrum of the PS-5CB (70:30) mixture, the following simple assumption was made: at a given glass transition temperature, a plasticizer plays a similar role on the free volume to that of the temperature. To compare the relaxation rate values of the high frequency mechanism observed for PS-5CB (70:30) with those of the α process reported in the literature for pure PS, we assumed that a shift of $\Delta T = T_g(\text{PS}) - T_g(\text{PS-5CB}) \sim 80^\circ\text{C}$ for a plasticized PS is approximately comparable to an increase in temperature of the same range above T_g for a pure PS of similar macromolecular weight M_w . The evolution of the peak frequency of dielectric loss due to the α process as a function of the inverse of temperature was simulated from experimental data reported by Fukao and Miyamoto [36,37] for thin PS films according to the Volger-Fulcher-Tammann (VFT) equation which is widely used to describe the temperature dependence of the relaxation frequency $1/\tau_{max}^\alpha$ of the α process:

$$\frac{1}{\tau_{max}^\alpha} = \frac{1}{\tau_0} \exp\left(\frac{-U}{T-T_V}\right), \quad (4)$$

where U is the apparent activation energy, T_V is the Vogel temperature, and $1/\tau_0$ is the relaxation frequency at high temperatures [38]. In Fig. 5, the \square , \triangleright , and \star symbols are data obtained in Refs. [36,37] for PS thin films, whereas the solid line is the VFT curve simulated from these data using Eq. (4) ($1/\tau_0 = 10^{9.31}$, $U = 297.3 \text{ J mol}^{-1}$, $T_V = 370.2 \text{ K}$). The \circ symbol corresponds to $1/\tau_{max}^\alpha$ values retrieved from the dielectric spectra of the PS-5CB (70:30) mixture. The relative agreement observed between the simulated VFT curve and the relaxation rates of the PS-5CB (70:30) blend seems

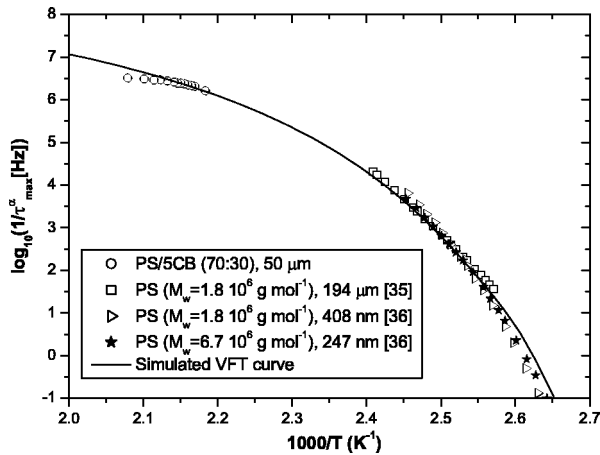
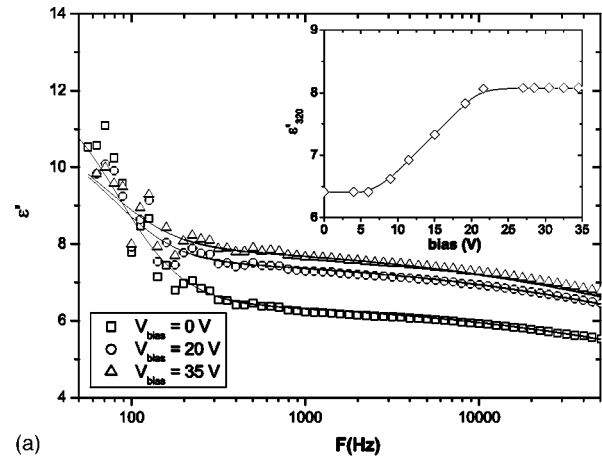


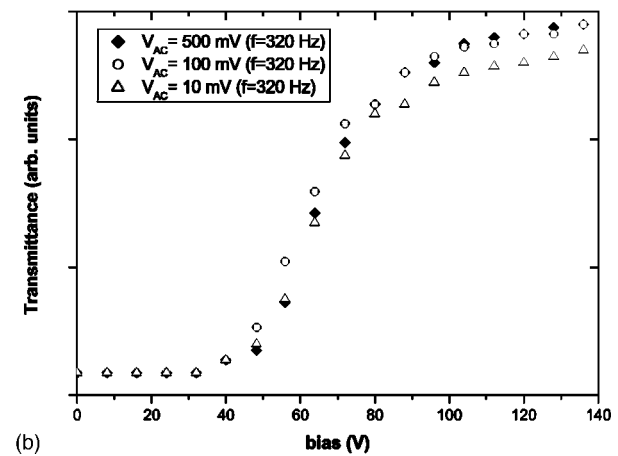
FIG. 5. Relaxation rate frequency of dielectric loss due to the α process as a function of the inverse of temperature for PS and PS-5CB (70:30) thin films, respectively. The solid curve is a simulation using Eq. 4.

to indicate that the high frequency relaxation mechanism can be correlated to the α process above T_g . Due to the strong plasticizing effect of 5CB molecules, the peak frequency is increased by at least two orders of magnitude compared with that of pure PS. The apparent activation energy is little temperature dependent indicating that the segmental motion of the macromolecular chains is mostly improved by the increase in the free volume induced by the dissolved LC molecules. Finally, the dielectric loss values due to α process reported by Fukao *et al.* are in the order of $\epsilon''_{max} \approx 0.8$ which is very close to the values presented in this work ($\epsilon''_{max} \approx 0.5$). Therefore, the high frequency relaxation process observed in the dielectric spectrum of the PS-5CB (70:30) mixture can be mainly related to the segmental motion of PS chains above T_g . Due to the overlapping with the α process and the small amplitude of the dielectric loss of the in-plane rotation along the long molecular axis of the LC molecules, this relaxation mechanism was not clearly evidenced.

In the case of the PS-5CB (30:70) system, two relaxation processes can be easily distinguished in the dielectric spectrum: the first one occurs at low frequency (~ 200 Hz) with a high dielectric strength, whereas the second one is detected at high frequency ($\sim 6-8$ MHz) with a lower $\Delta\epsilon$. Compared with the PS-5CB (70:30) system, the dielectric spectrum of the PS-5CB (30:70) mixture exhibits a drastic difference in the low frequency region. In order to understand this behavior, it is helpful to consider the phase diagram of the PS-5CB system. At $T=25^\circ\text{C}$, one can clearly see that the PS-5CB (30:70) blend exhibits a morphology consisting of phase-separated nematic droplets dispersed in an isotropic polymer-rich phase (see Figs. 1 and 2). This kind of morphology, characterizing a heterogeneous mixture, can be compared to a dispersion of spherical or ellipsoidal domains of component "a," i.e., the LC rich phase, in a continuous medium "b," i.e., the polymer-rich phase. For a heterogeneous mixture of two or more components the accumulation of charges at the interfaces between phases gives rise to polarization which contributes to relaxation if at least one component has nonzero electric conductivity. The phenomenon is



(a)



(b)

FIG. 6. Influence of the applied dc bias voltage on the real (ϵ') part of the complex permittivity of a $50\ \mu\text{m}$ thick PS-5CB (30:70) film in the frequency range 50 Hz–50 kHz at $T=25^\circ\text{C}$ [top (a)]; inset: evolution of ϵ' at 320 Hz as a function of the applied bias voltage. Evolution of the transmittance of the same film as a function of applied dc bias voltage for three different oscillating (ac) signals [bottom (b)].

known as the Maxwell-Wagner-Sillars (MWS) effect [17,27,34]. The MWS effect originates from restricted motion of charge carriers in the cavities, and, due to its slow relaxation process, this mechanism is observed in the low frequency region of the dielectric spectrum [22]. If a MWS effect occurs at ~ 200 Hz for the PS-5CB (30:70) system, its dielectric response should be modified upon application of a bias voltage V_{bias} . Figure 6 displays the frequency dependence (50 Hz–50 kHz) of the real part (ϵ') of the complex permittivity for three different applied dc bias voltages ($V_{bias}=0, 20, 35$ V). It clearly appears that increasing V_{bias} leads to an increase in ϵ_∞ whereas ϵ_s remains nearly constant at ~ 11 . This behavior is clearly evidenced in the inset of Fig. 6 where the evolution of ϵ' measured at a given frequency (320 Hz) is displayed as a function of applied bias voltage. This result can be explained by the fact that the number of dipoles associated with the electrical charges located at the droplet interfaces are further aligned along the bias field with increasing V_{bias} until leveled off. Therefore the application of a bias voltage leads to a decrease in am-

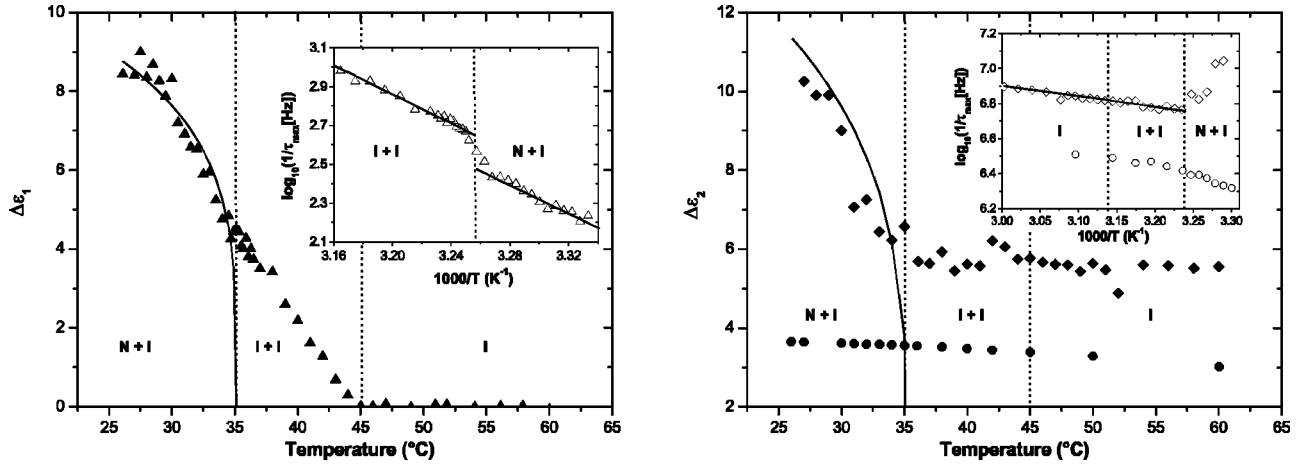


FIG. 7. Temperature dependence of the dielectric strengths $\Delta\epsilon_1$ (\blacktriangle) for the low frequency relaxation process observed in confined 5CB [PS-5CB (30:70)] (left), and $\Delta\epsilon_2$ for the high frequency mechanism (right) detected for PS-5CB (30:70) (\blacklozenge) and PS-5CB (70:30) mixtures (\bullet), respectively (film thickness $50\ \mu\text{m}$). The solid lines are Haller-type fit curves. Insets: Arrhenius plot of the temperature dependence of the relaxation rate $1/\tau_{max}$ for the corresponding processes [(\triangle) , $1/\tau_{max}$ of the PS-5CB (30:70) low frequency process, (\diamond), $1/\tau_{max}$ of the PS-5CB (30:70) high frequency process, and (\circ), $1/\tau_{max}$ of the PS-5CB (70:30) high frequency process].

plitude of the low frequency relaxation mechanism. However, the application of a bias voltage of sufficient magnitude might also reorient the liquid crystal director field in the droplets and raise the effective dielectric constant. In order to determine if such a phenomenon occurs, the transmittance of the same $50\ \mu\text{m}$ thick film was recorded at 320 Hz as a function of the applied field which was set identical to that generated by the impedance or gain-phase analyzer. In Fig. 6 [bottom (b)], one can see that the application of a dc bias voltage upon the oscillating signal (320 Hz) does not change the transmission properties of the PS-5CB film up to 35 V. This observation clearly indicates that in the bias range where ϵ' varies the field strength is not sufficient to reorient the LC director field inside the droplets, whatever the amplitude of the oscillating signal used, i.e., 10, 100, or 500 mV. It can be then reasonably assumed that the slow relaxation process observed at ~ 200 Hz for the PS-5CB (30:70) system is mostly related to an interfacial polarization (MWS) effect which can lead to a depolarization process across the PDLC film.

The high frequency relaxation process observed at ~ 7 MHz may originate from the 5CB molecules and the PS chains. Indeed, it should be kept in mind that in the case of PS-5CB (30:70) a fraction of the LC content is phase separated in nematic droplets, while the other part remains dissolved in the polymer-rich phase. Different relaxation mechanisms may then arise because the segregated LC molecules behave as pure 5CB, as evidenced in Sec. III A, whereas the dissolved 5CB molecules can be considered as single molecules randomly dispersed in an isotropic viscous polymeric medium. For this second case, similar relaxation mechanisms as that of PS-5CB (70:30) are expected meaning that the α process above T_g obviously contributes to the fast relaxation process. Concerning the phase-separated LC molecules, the assignment of the various high frequency relaxation processes was based on previous investigations of cyanobiphenyl derivatives in bulk and cavities [10,17,22,24,39–41]. In the nematic phase, two processes

can contribute to the dielectric response: the first one (slow, $\sim 10^7$ Hz) originates from 180° flips about the molecular short axis, and the second one (fast, $\sim 10^9$) is connected with the tumbling of the molecular long axis around the local director \mathbf{n} . Taking into account the investigated frequency range (50 Hz–13 MHz), the relaxation process observed at ~ 7 MHz corresponds to the rotation of the 5CB molecules around their molecular short axis. In the isotropic phase, these two contributions become one which is assigned to isotropic reorientation of the molecular long axis. In addition to these mechanisms, another process may arise due to anchored molecules at the polymer-LC interface which are in rapid exchange with free molecules in the LC droplets ($\sim 10^6$ Hz) [8,22]. The high frequency relaxation process observed in the dielectric spectra of PS-5CB system is probably a combination of the various mechanisms, i.e., rotation around the molecular short axis (5CB), rapid exchange of the anchored molecules with free molecules (5CB), and α process (PS). Unfortunately, we were not able to determine and assign with satisfactory precision each mechanism due to their close relaxation rates (overlapped processes) and limitations in our experimental setup above 10 MHz. However, it should be noted that compared to low frequency relaxation mechanisms, high frequency processes have less influence on the electro-optical performances of PDLC-based display devices which are usually driven by 50–100 Hz electric fields (i.e., close to domestic household ac voltage frequencies).

In Fig. 7, the temperature dependence of the dielectric strengths $\Delta\epsilon$ and the corresponding relaxation rates $1/\tau_{max}$ (insets) are shown for both low (left, $\Delta\epsilon_1$) and high (right, $\Delta\epsilon_2$) frequency processes, respectively. In the (N+I) region, the evolution of $\Delta\epsilon$ can be correlated with the behavior of the nematic order parameter S according to the Haller equation [8,41,42]

$$\Delta\epsilon \propto S = S_0 \left(1 - \frac{T}{T_{NI}} \right)^F, \quad (5)$$

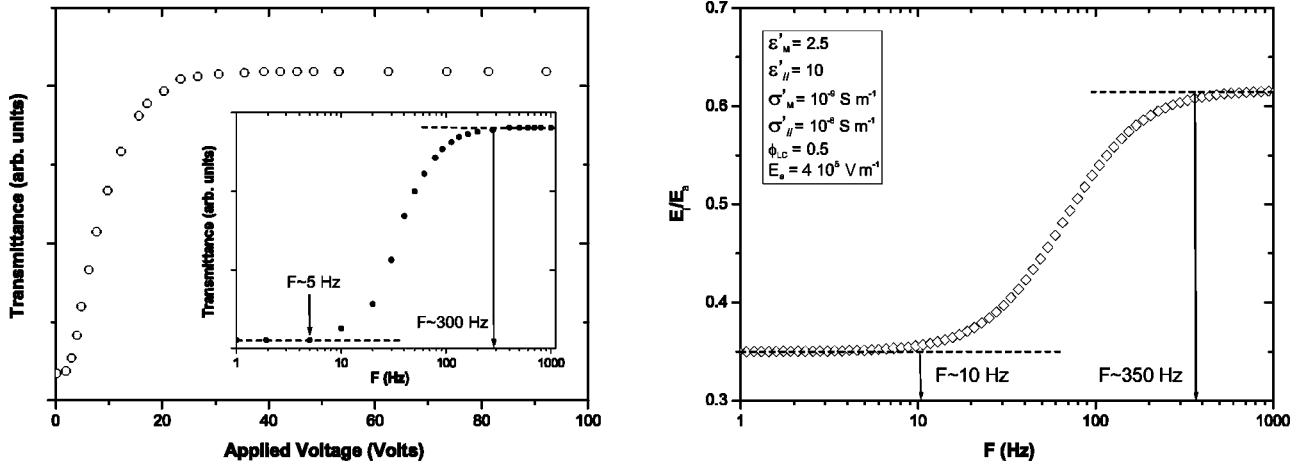


FIG. 8. Evolution of the transmittance vs applied voltage at 1 kHz of a 50 μm thick PS-5CB (30:70) film (left); inset: frequency dependence of the transmittance at $V=20$ V. Simulation [Eq. (6)] of the field inside a spherical droplet (E_i) over sinusoidal applied field (E_a) as a function of frequency (right).

where S_0 is the limit of the order parameter with decreasing temperature, and F may be considered as an indication of how quickly a molecular segment reaches the limit of the order parameter as a function of change in temperature. The solid lines in Fig. 7 are the best fit curves using Eq. (5). The factor F which describes how fast S changes with temperature was found in the order of 0.25 for both mechanisms. This value is in good agreement with those reported in the literature for confined 5CB [8]. As we can see in Fig. 7, $\Delta\epsilon_1$ and $\Delta\epsilon_2$ exhibit completely different behaviors in the $I+I$ and I regions. In the case of the low frequency mechanism, $\Delta\epsilon_1$ follows a linear decrease with increasing temperature until it becomes null when the sample reaches the I state. The linear decrease of $\Delta\epsilon_1$ can be explained by the diminution of the density number of isotropic LC droplets with increasing temperature due to an improved miscibility between the LC and the polymer at high temperature [43,44]. The fact that $\Delta\epsilon_1$ is null above the $(I+I)$ to (I) transition temperature ($T_{(I+I)-(I)}$) is a clear indication of the close relationship between the low frequency relaxation process and the sample morphology. Indeed this is in good agreement with the assumption based on polarization effects at the polymer-LC droplet interfaces which vanish when the sample becomes homogeneous in the (I) domain. Moreover, the temperature dependence of the mean relaxation rate $1/\tau_{max}$ (inset of Fig. 7, left) is another factor indicating again that a MWS effect occurs. The evolution of $\log_{10}(1/\tau_{max})$ versus $1/T$ exhibits an Arrhenius-like behavior in both $(N+I)$ and $(I+I)$ regions except in the vicinity of $T_{(N+I)-(I+I)}$ where a shift is observed. This shift can be explained by the drastic changes in the nematic order parameter S at the $N-I$ transition (first order transition) which affect the homogeneous anchoring of 5CB at the PS interface [45] leading to variations in the relaxation rates of interfacial polarization effects at T_{NI} . The activation energies E_A^{MWS} retrieved from the relaxation rate data were found in the same range in the $(N+I)$ and $(I+I)$ domains, i.e, 68.1 kJ mol^{-1} , and 61.9 kJ mol^{-1} , respectively. These small but distinct differences in E_A^{MWS} show again that the nematic order and the LC anchoring conditions

influence the MWS effect which is enhanced when the LC phase is in the isotropic state. Finally, the calculated E_A^{MWS} values are in agreement with those reported by Perrier and Bergeret who found MWS activation energies in the range of 80 kJ mol^{-1} for PS-glass beads composites [27]. In the case of the high frequency mechanism, the sample morphology does not seem to influence the relaxation process because $\Delta\epsilon_2$ is almost constant in both $(I+I)$ and (I) states. The value of $\Delta\epsilon_2$ is in the order of ~ 6 , which is close to that of isotropic bulk 5CB ($\Delta\epsilon \sim 6.5$) assigned to the reorientation of the molecular long axis at 10 MHz [22,40,46]. The fact that $\Delta\epsilon_2$ remains nearly unchanged even in the (I) region (homogeneous mixture) indicates that “solite” (LC) concentration effects [35] occur due to the high 5CB content (70 wt %). Therefore the relaxation mechanism associated with the 5CB molecules in the I state is predominant compared to the α process above T_g of PS chains. For the sake of comparison the dielectric strength $\Delta\epsilon_2$ and the relaxation rate $1/\tau_{max}$ of the fast process obtained for the PS-5CB (70:30) mixture are also represented in Fig. 7 by \bullet and \circ symbols, respectively. One can clearly see that $\Delta\epsilon_2$ remains nearly constant in the temperature range of interest (25–60 $^\circ\text{C}$) confirming that this relaxation process is mostly related to the segmental motion of PS chains rather than to a mechanism associated with LC molecules.

C. Electro-optical properties

In order to correlate the dielectric properties of PS-5CB mixtures with their EO behavior, transmittance versus applied voltage measurements have been carried out on PS-5CB (30:70) films. Upon application of an external sinusoidal field (1 kHz) the LC molecules inside the droplets reorient leading to a typical sigmoidal curve shape plot for the transmittance [Fig. 8 (left), \circ symbol] [1,31]. Using the self consistent field approximation, the field inside a spherical droplet E_i can be estimated for a sinusoidal applied field [25,34,47]:

$$E_i(\omega) = \frac{3\epsilon_M^*}{\epsilon_{LC}^* + 2\epsilon_M^* - \phi_{LC}(\epsilon_{LC}^* - \epsilon_M^*)} E_a \exp(-j\omega t), \quad (6)$$

where ϕ_{LC} is the phase-separated LC fraction ($\phi_{LC} \sim 0.5$ according to the inset of Fig. 3), E_a is the magnitude of the applied field ($E_a = V_a/d$), and

$$\epsilon_M^* = \epsilon'_M - j \frac{\sigma'_M}{\omega \epsilon_0}, \quad (7)$$

$$\epsilon_{LC}^* = \epsilon'_{\parallel} - j \frac{\sigma'_{\parallel}}{\omega \epsilon_0}, \quad (8)$$

where ϵ'_M and ϵ'_{\parallel} are the dielectric permittivities of the PS matrix and LC aligned along E_a , respectively, and σ'_M and σ'_{\parallel} are the electrical conductivities of the PS matrix and LC aligned along E_a , respectively. Figure 8 shows a simulated curve of E_i/E_a versus frequency using Eq. (6) with $\epsilon'_M = 2.5$ [27], $\epsilon'_{\parallel} = 10$ [46], $\sigma'_M = 10^{-9} \text{ S m}^{-1}$ [27], $\sigma'_{\parallel} = 10^{-8} \text{ S m}^{-1}$ [26], $V_a = 20 \text{ V}$, and $d = 50 \times 10^{-6} \text{ m}$. One can see that starting from $\sim 350 \text{ Hz}$ E_i/E_a decreases and tends to a constant value below $\sim 10 \text{ Hz}$. This behavior can be explained by the presence of charges located at the polymer-LC interfaces (MWS effect) which will move under the influence of the external field (conductivity effect), setting up a depolarization field across the film. At high frequencies, conductivity effects become unimportant relative to dielectric effects because the charge motion is frozen out. In comparison, conductivity effects dominate the dielectric terms at low frequency leading to a depolarization field which will tend to cancel the applied field ($F < 10 \text{ Hz}$). According to this simulation, it is expected that the transmittance of PS-5CB films will vary by using appropriate driving field frequencies. In order to correlate this prediction with experiments, the sinusoidal voltage applied across the film was set at $V_a = 20 \text{ V}$, so that the film exhibits a maximum transmittance (T_{max}), then the frequency was varied from 1 kHz to 1 Hz. As shown in the inset of Fig. 8 (left, ● symbol), T_{max} decreases with decreasing frequency. The frequency range to switch the film from a transparent to a scattering state (300–5 Hz) is in good agreement with the simulation of E_i/E_a versus F where E_i/E_a drops from a maximum to a minimum value for F ranging from 350 to 10 Hz. This result is also in good agreement with the low frequency absorption domain detected in the dielectric spectra at $\sim 200 \text{ Hz}$. The strong frequency dependence ($5 < F < 300 \text{ Hz}$) of the transmittance properties drastically influences the operation of PS-5CB devices through a depolarization field which is obviously related to the accumulation of charges at the polymer-LC interfaces (MWS effect). The correlation between the internal droplet field and the transmittance properties of PS-5CB (30:70) films also confirms the ability to drive PDLC films by applying sinusoidal voltages of suitable frequencies.

D. Discussion

The comparison between the electro-optical efficiency of dc (Fig. 6) and ac (Fig. 8) driving fields clearly shows that threshold (V_{10}) and saturation (V_{90}) voltages required to drive the same PDLC film are at least five times larger for dc signals compared to ac ones. This behavior is obviously related to a depolarization field associated with a MWS effect as evidenced in Secs. III B and III C. The nature of the depolarization field depends on the relative conductivity of polymer and liquid crystal. Erdmann *et al.* reported for epoxy-based PDLC that a linear relationship exists between the saturation voltage (V_{90}) and the polymer resistivity [48]. In other words, when the polymer conductivity σ decreases, the liquid crystal reorientation field increases. In the case of PS-5CB mixtures, $\sigma_{ac}(\text{PS}) \gg \sigma_{dc}(\text{PS})$ (see Sec. II) which implies, according to Erdmann *et al.*, that $V_{90}^{dc} \gg V_{90}^{ac}$. This is in good agreement with our experimental observations meaning that our model system obeys a similar law to that reported for epoxy-based PDLC.

The conductivity is relative and depends on the applied frequency. Film conductivity effects are invariably suppressed at high enough frequencies whereas they can dominate the dielectric terms at low frequencies and low resistivities. For low frequencies, Kelly and Seekola pointed out that the field inside a spherical droplet [Eq. (6)] reduces to [47]

$$E_i(\omega \rightarrow 0) = \frac{3\sigma_M}{\sigma_{LC} + 2\sigma_M - \phi_{LC}(\sigma_{LC} - \sigma_M)} E_a \exp(-j\omega t), \quad (9)$$

where σ_M and σ_{LC} are the conductivities of the polymer matrix and liquid crystal, respectively. It is apparent from this expression that when the LC conductivity is much greater than the matrix conductivity ($\sigma_{LC} \gg \sigma_M$), then $E_i \approx 0$. In the case of the PS-5CB system, $\sigma_{5CB} \gg \sigma_{PS}$ implying $E_i \approx 0$ for a dc field. However, as displayed in Fig. 6 (right), application of a high dc field strength allows to switch the PDLC film from an opaque to a transparent state. The discrepancy between experimental results and semiempirical predictions probably arises from the fact that the LC solubility limit in the polymer matrix is high ($\beta \sim 55\%$, see Sec. III A) leading to a substantial increase in the polymer conductivity. Therefore, the condition requiring $\sigma_{LC} \gg \sigma_M$ is not strictly verified and then $E_i \neq 0$.

Instead of the above semiempirical equations, Bucci and Golemme reported sophisticated numerical calculations of the electric field across an isolated nematic droplet suspended in an isotropic medium [49]. These authors demonstrated that when $\sigma_{LC} > \sigma_M$, the field is strong across the interfacial region and low within the droplet volume, consistent with the effect of depolarization charges reducing the field across the droplet cavity. Recalling that $\sigma_{5CB} > \sigma_{PS}$, the electrical behavior of the PS-5CB mixtures is then in good agreement with the numerical calculations of Bucci and Golemme confirming that a MWS effect occurs at the polymer-LC interfaces which reduces E_i .

The numerous papers discussing depolarization field effects in PDLC combined to the results of this work demon-

strate that this phenomenon strongly affects the electro-optical performances of PDLC materials which can even be detrimental to technological developments for some polymer-LC formulations. One way to overcome this drawback has been reported by De Filipo *et al.* who showed that the application of a precharging dc bias voltage counteracts the inner polarization field improving the electro-optical response of a PMMA-E49 mixture [50].

IV. CONCLUSION

The thermophysical, dielectric, and electro-optic properties of PDLC films made of monodisperse PS and 5CB were investigated by polarized optical microscopy, differential scanning calorimetry, ac impedance analysis, and forward transmittance measurement technique. The phase diagram of the PS-5CB system exhibits an UCST shape with four distinct regions: a single isotropic phase, and three biphasic regions (isotropic+isotropic), (nematic+isotropic), and (crystal+isotropic). The drastic variation of the polymer glass transition temperature T_g as a function of the composition of 5CB indicates that the LC plays the role of plasticizer for the polymer matrix. The solubility limit β of the LC molecules in the polymer and the relative amount δ of LC in the nematic droplets were also deduced from the phase diagram and the thermodynamic quantities accessible from DSC data. The real (ϵ') and imaginary (ϵ'') parts of the complex permittivity of the PS-5CB (30:70) and PS-5CB (70:30) mixtures were investigated in the frequency range 50 Hz–10 MHz. In the case of the PS-5CB (70:30) system, a relaxation mechanism is observed at high frequency ~ 4 –6 MHz which was correlated to the α process above T_g due to the plasticizing effect of LC and the relative agreement observed between the simulated VFT curve and the experimental relaxation rates. In the case of the PS-5CB (30:70) system, two relaxation processes were distinguished in the dielectric

spectrum. The slow relaxation process observed at ~ 200 Hz was related to an interfacial polarization (MWS) effect. The high frequency relaxation process observed at ~ 7 MHz probably originates from a combination of various mechanisms, i.e., rotation around the molecular short axis (5CB), rapid exchange of the anchored molecules with free molecules (5CB), and α process (PS). The temperature dependence of the dielectric strengths $\Delta\epsilon$ and the corresponding relaxation rates $1/\tau_{max}$ were determined by using the Havriliak-Negami analysis. In the $(N+I)$ region, the behavior of $\Delta\epsilon$ of PS-5CB (30:70) was associated with the thermal evolution of the nematic order parameter S . It has also been shown that the low frequency relaxation process is closely related to the sample morphology. The evolution of $\log_{10}(1/\tau_{max})$ versus $1/T$ exhibits an Arrhenius-like behavior in both $(N+I)$ and $(I+I)$ regions confirming that a MWS effect occurs. Using the self-consistent field approximation, the field inside a spherical droplet E_i was simulated for a sinusoidal applied field, showing an important decrease in the frequency range 350–10 Hz. This behavior was explained by the influence of a depolarization field across the film resulting from the presence of charges located at the polymer-LC interfaces (MWS effect). Experimentally, the frequency range to switch the film from a transparent to a scattering state (300–5 Hz) was in good agreement with the simulation and the low frequency absorption domain observed in the dielectric spectra confirming that the field frequency drastically influences the operation of PS-5CB devices.

ACKNOWLEDGMENTS

The authors are indebted to the EU program Interreg III, the MJENR, and the CNRS for financial support. Professor J.M. Buisine and Professor C. Legrand are kindly acknowledged for helpful discussions.

-
- [1] P. S. Drzaic, *Liquid Crystals Dispersions* (World Scientific, Singapore, 1995).
- [2] G. P. Crawford and S. Žumer, *Liquid Crystals in Complex Geometries* (Taylor and Francis, London, 1996).
- [3] D.A. Higgins, *Adv. Mater.* (Weinheim, Ger.) **12**, 251 (2000).
- [4] S. M. Kelly and M. O'Neill, in *Handbook of Advanced Electronics and Photonic Materials and Devices*, edited by H. S. Nalwa (Academic Press, Boston, 2000), Vol. 7, p. 1.
- [5] K. Amundson, A. van Blaaderen, and P. Wiltzius, *Phys. Rev. E* **55**, 1646 (1997).
- [6] K.R. Amundson and M. Srinivasarao, *Phys. Rev. E* **58**, R1211 (1998).
- [7] J. Zhou, D.M. Collard, J.O. Park, and M. Srinivasarao, *J. Am. Chem. Soc.* **124**, 9980 (2002).
- [8] F. Roussel, C. Canlet, and B.M. Fung, *Phys. Rev. E* **65**, 021701 (2002); F. Roussel and B.M. Fung, *ibid.* **67**, 041709 (2003).
- [9] K.R. Amundson, *Phys. Rev. E* **58**, 3273 (1998); **59**, 1808 (1999).
- [10] J. Jadżyn, G. Czechowsky, M. Mucha, and E. Nastał, *Liq. Cryst.* **26**, 453 (1999).
- [11] C. Serbutoviez, J.G. Kloosterboer, H.M.J. Boots, and F.J. Touwslager, *Macromolecules* **29**, 7690 (1996).
- [12] J.B. Nephew, T.C. Nihei, and S.A. Carter, *Phys. Rev. Lett.* **80**, 3276 (1998).
- [13] F. Roussel *et al.*, *Phys. Rev. E* **62**, 2310 (2000); **65**, 011706 (2002).
- [14] J.R. Kelly and P. Palfy-Muhoray, *Mol. Cryst. Liq. Cryst.* **243**, 11 (1994).
- [15] O. Levy, *Phys. Rev. E* **61**, 5385 (2000); *Eur. Phys. J. E* **3**, 11 (2000).
- [16] V.Y. Reshetnyak, T.J. Sluckin, and S.J. Cox, *J. Phys. D* **29**, 2459 (1996); **30**, 3253 (1997).
- [17] F. Kremer and A. Schönhals, *Broadband Dielectric Spectroscopy* (Springer-Verlag, Berlin, 2003).
- [18] G.P. Crawford, R. Stannarius, and J.W. Doane, *Phys. Rev. A* **44**, 2558 (1991).
- [19] G.P. Crawford, D.W. Allender, and J.W. Doane, *Phys. Rev. A* **45**, 8693 (1992).
- [20] G.S. Iannachione, G.P. Crawford, S. Žumer, J.W. Doane, and D. Finotello, *Phys. Rev. Lett.* **71**, 2595 (1993).

- [21] T. Bellini, N.A. Clark, and D.W. Schaefer, *Phys. Rev. Lett.* **74**, 2740 (1995).
- [22] C. Cramer, T. Cramer, F. Kremer, and R. Stannarius, *J. Chem. Phys.* **106**, 3730 (1997).
- [23] F. M. Aliev, in *Liquid Crystals in Complex Geometries*, edited by G. P. Crawford and S. Žumer (Taylor and Francis, London, 1996), p. 345.
- [24] A. Hourri, T.K. Bose, and J. Thoen, *Phys. Rev. E* **63**, 051702 (2001); A. Hourri, P. Jamée, T.K. Bose, and J. Thoen, *Liq. Cryst.* **3**, 459 (2002).
- [25] D. L. Seekola, Ph.D. thesis, Kent State University, Kent, OH, 1992.
- [26] V. Allouchery, Ph. D. Thesis, Université du Littoral-Côte d'Opale, France, 2000 (unpublished).
- [27] G. Perrier and A. Bergeret, *J. Appl. Phys.* **77**, 2651 (1995).
- [28] D.R. Lide, *Handbook of Chemistry and Physics* (CRC Press, New York, 1997).
- [29] W. Ahn, C.Y. Kim, H. Kim, and S.C. Kim, *Macromolecules* **25**, 5002 (1992).
- [30] F. Benmouna *et al.*, *J. Polym. Sci., Part B: Polym. Phys. Ed.* **37**, 1841 (1999); *Macromolecules* **33**, 960 (2000).
- [31] F. Roussel, R. Chan Yu King, and J.-M. Buisine, *Eur. Phys. J. E* **11**, 293 (2003).
- [32] G.W. Smith and N.A. Vaz, *Liq. Cryst.* **3**, 543 (1988); G.W. Smith, *Mol. Cryst. Liq. Cryst.* **180**, 201 (1990).
- [33] S. Havriliak and S. Negami, *J. Polym. Sci., Part C: Polym. Symp.* **14**, 99 (1966); *Polymer* **8**, 161 (1967).
- [34] B. K. P. Scaife, *Principles of Dielectrics* (Clarendon Press, Oxford, 1989).
- [35] S.P. Tay and S. Walker, *J. Chem. Phys.* **63**, 1634 (1975); H. A Khwaja and S. Walker, *Adv. Mol. Relax. Interact. Processes* **19**, 1 (1981).
- [36] K. Fukao and Y. Miyamoto, *Phys. Rev. E* **61**, 1743 (2000).
- [37] K. Fukao and Y. Miyamoto, *Phys. Rev. E* **64**, 011803 (2001).
- [38] H. Vogel, *Phys. Z.* **22**, 645 (1921); G.S. Fulcher, *J. Am. Ceram. Soc.* **8**, 339 (1925).
- [39] J. Jadzyn, G. Czechowsky, R. Douali, and C. Legrand, *Liq. Cryst.* **26**, 1591 (1999).
- [40] S. Rozanski, R. Stannarius, H. Groothues, and F. Kremer, *Liq. Cryst.* **20**, 59 (1996).
- [41] S.J. Rzoska, J. Ziolo, W. Sułkowski, J. Jadzyn, and G. Czechowsky, *Phys. Rev. E* **64**, 052701 (2001).
- [42] I. Haller, *Prog. Solid State Chem.* **10**, 103 (1975).
- [43] G. De Filpo, J. Lanzo, F.P. Nicoletta, and G. Chidichimo, *J. Appl. Phys.* **85**, 2894 (1999); J. Lanzo, F.P. Nicoletta, G. De Filpo, and G. Chidichimo, *Liq. Cryst.* **27**, 1029 (2000).
- [44] N. Gogibus, Ph.D. thesis, Université des Sciences et Technologies de Lille, France, 2001 (unpublished).
- [45] M. Oh-e, S.-C. Hong, and Y.R. Shen, *Appl. Phys. Lett.* **80**, 784 (2002).
- [46] B. Gestblom and S. Wróbel, *Liq. Cryst.* **18**, 31 (1995).
- [47] J. Kelly and D. Seekola, *Proc. SPIE* **1257**, 17 (1990).
- [48] J. Erdmann, J.W. Doane, S. Žumer, and G. Chidichimo, *Proc. SPIE* **1080**, 32 (1989).
- [49] P. Bucci and A. Golemme, *J. Chem. Phys.* **98**, 10070 (1993).
- [50] G. De Filpo, Z. Huang, G. Chidichimo, and D. Imbardelli, *Mol. Cryst. Liq. Cryst.* **304**, 71 (1997).